Journal of Geochemical Exploration 209 (2020) 106438

Contents lists available at ScienceDirect

Journal of Geochemical Exploration

journal homepage: www.elsevier.com/locate/gexplo

Anthropic-induced salinization in a dolomite coastal aquifer. Hydrogeochemical processes

A. Vallejos[a,*], L. Daniele[b,c], F. Sola[a], L. Molina[a], A. Pulido-Bosch[a,d]

[a] Water Resources and Environmental Geology, University of Almería, Spain
[b] Department of Geology, FCFM, University of Chile, Chile
[c] Andean Geothermal Center of Excellence (CEGA), Fondap-Conicyt, Chile
[d] Department of Geodynamics, University of Granada, Spain

ARTICLE INFO

Keywords:
Carbonate aquifer
Marine intrusion
Cationic exchange
Dolomitization

ABSTRACT

The dolomite coastal aquifer of Balanegra (SE Spain) is the only source of irrigation water in an area of flourishing intensive agriculture. This scenario has consequently led to a severe exploitation of the water resources. This aquifer extends from the edges of the Sierra de Gádor to the sea, deepening progressively under the thick Neogene sedimentary sequence that confines it. Based on the content of major ions, the groundwater was classified into four groups (G1 to G4). G1 samples were characterized by their high content of dominating ions HCO_3^- and Mg^{2+}. Samples classified as G2 showed a similar composition, but with a higher SO_4^{2-} ion content. As for samples corresponding to groups G3 and G4, they were characterized by their chloride content. However, Na^+ is the major cation in G3 and Mg^{2+} in G4.

Based on the study of ionic relationships, ionic deltas and mineral saturation indices, it was possible to elucidate the main processes that condition the chemical composition of each of these groups of samples. The most important among said processes is the dissolution of dolomite or dolomitic limestone, the primary component of the aquifer rock. Compositional changes are due to SO_4^{2-} concentration resulting from gypsum dissolution (G2). In G3, salinity is the result of dissolution of salts, or contamination through saline waters of the upper detrital aquifer. Seawater intrusion, a consequence of the overexploitation of the aquifer, increases the salinity in the G4 samples. In this intrusion process, waters of marine origin rich in Mg, interact with the carbonated rock, favouring a cation exchange in which Mg is fixed in dolomite or dolomitic limestone and Ca ion is released. This process is supported by the ionic delta values of these two cations. The marine intrusion in the area is facilitated through groundwater overexploitation, and also by the structuring of the aquifer. Marine intrusion exists where tectonics has allowed interconnection between the carbonate rock and the sea. In other areas on this coast, marine intrusion has not been possible because of the presence of impermeable Neogene materials that prevent this interconnection.

1. Introduction

One of the major threats to coastal aquifers is the aquifer salinization due to seawater intrusion, yet it also constitutes an early warning sign of such an event at a specific point in time and space, which can prove invaluable to water authorities around the world (Russak and Sivan, 2010; Ferguson and Gleeson, 2012; Werner et al., 2013; Colombani et al., 2016). These coastal zones and adjacent land areas support 60% of the human population and eight of the top-10 largest cities in the world (González-Baheza and Arizpe, 2018). In addition, coastal areas usually enjoy a more benign microclimate that favours the practice of agricultural activities and, as a result, they feature a high concentration of large irrigated areas. Both the presence of humans and human activities require a substantial contribution of water to ensure their sustainability. In arid or semi-arid areas, the scarcity of superficial water resources is a problematic characteristic that can compromise the future development of such regions (Burak et al., 2004). In these cases, groundwater is often the solution to this water deficit, inevitably resulting in overexploitation of its aquifers (Changming et al., 2001; Gorelick and Zheng, 2015; Custodio et al., 2016).

Freshwater extraction of coastal aquifers that have a hydraulic connection with seawater leads to the salinization of these water sources by advancing the saline wedge towards the continent and through “up-coning” generated under the extraction wells (Werner

* Corresponding author.
E-mail address: avallejo@ual.es (A. Vallejos).

https://doi.org/10.1016/j.gexplo.2019.106438
Received 29 May 2019; Received in revised form 15 November 2019; Accepted 1 December 2019
Available online 06 December 2019
0375-6742/

et al., 2009, 2012). A seawater content of 3% can render the water too salty for many uses, and 5% practically renders it useless, that is unless very expensive desalinating processes are implemented (Custodio and Bruggeman, 1987). Nevertheless, not all coastal aquifers displaying high salinity values owe their high salt content to processes linked to marine intrusion. Other human activities such as groundwater abstraction, agricultural irrigation or wastewater disposal, as well as natural factors, can cause the progressive increase in the salinity of groundwater (Pulido-Bosch et al., 2018). Several studies have highlighted high groundwater salinity as a consequence of natural interactions between matrix rock and groundwater (Daniele et al., 2013; Mollema et al., 2013; Carreira et al., 2014), or as a result of its geological history (Edmunds, 2001; Raidla et al., 2009; Sola et al., 2014; Cary et al., 2015; Vallejos et al., 2018). Marine aerosol input has also been considered as a potential source of increased salinization in aquifers near the coastline (Du et al., 2015; Chowdhury et al., 2018).

Knowing the origin of groundwater salinity is essential for the proper management of aquifers (Bear, 2004; Shi and Jiao, 2014; Scheiber et al., 2015; Pulido-Bosch et al., 2018). Numerous geophysical, hydrogeochemical and isotopic techniques have been proposed to determine the origin of groundwater salinization (Vengosh et al., 2005; Alcalá and Custodio, 2008; Tran et al., 2012; Yechieli et al., 2019). Environmental stable isotopes can allow the groundwater hydrodynamics in karstic aquifers to be defined (Barbieri et al., 2005; Vallejos et al., 2015) and the origin of salinity in coastal groundwater recognized (Gattacceca et al., 2009; Caschetto et al., 2016; Gomes et al., 2019). Hydrogeochemistry is the tool that has most commonly been used, mainly because of its high resolution capacity and relatively affordable cost. More specifically, the hydrogeochemistry techniques that have been most widely used are ionic ratios of major, minor and trace elements (Sukhija et al., 1996; Vengosh et al., 1999; Sánchez-Martos et al., 2002; Alcalá and Custodio, 2008), ionic deltas, mixing calculations (Sivan et al., 2005; Liu et al., 2017) and geochemical modeling (Pulido-Leboeuf, 2004; Sola et al., 2013). Moreover, to study the patterns and rates of dissolution in a coastal aquifer, combined reactive-transport/density-dependent flow models can been adopted (Campana and Fidelibus, 2015).

This paper discusses the geochemical processes that give rise to a wide range of hydrochemical facies in a coastal carbonate aquifer, composed primarily of dolomite rocks. The interaction between carbonate minerals and groundwater in carbonate aquifers has a strong influence on groundwater chemistry and the dissolution/precipitation reactions may be defined from variations in the groundwater chemical composition. By interpreting geochemical data from groundwater samples, this study will determine the possible origin(s) of the saline water.

2. Hydrogeological setting

The Campo de Dalías coastal plain is situated in the extreme southeast of Spain, covering an area of about 330 km^2 underlain by a geologically complex aquifer system. Its northern limit is in the foothills of the Sierra de Gádor, while its southern edge is formed by the Mediterranean Sea (Fig. 1). The semiarid character of the area is determined by a combination of low precipitation (about 260 mm/yr), strong insolation and interannual variability of precipitation. However, the neighbouring Sierra de Gador is wetter and naturally recharges the groundwater system of Campo de Dalias (Pulido-Bosch, 2005). Apart from geological and climatic features, the main anthropogenic stressor is agriculture with more than 20,000 ha of highly profitable early-season greenhouse crops grown in the study area.

The aquifers of the Campo de Dalías are grouped into three hydrogeological units (Fig. 1A): Aguadulce, Balerma-Las Marinas and Balanegra (Pulido-Bosch et al., 1992; Molina et al., 2002). The Balerma-Las Marinas unit, in the central part, is comprised of Pliocene calcarenites/conglomerates partially overlain by marine and continental Quaternary sediments; the Aguadulce unit (the easternmost of the three), consists of Permotriassic limestone-dolomitic deposits, Miocene calcarenites, Pliocene calcarenites and Quaternary deposits. The Balanegra unit, at the western end of the Campo de Dalías, lies partly beneath the Balerma-Las Marinas aquifer, separated from the latter by the Pliocene marls, which act as the confining upper strata. The Balanegra unit is essentially comprised of Triassic carbonate materials. The structure of the aquifer is controlled by the tectonics. The dolomite basement is folded in a kilometric scale synclinal filled with detrital Neogene sediments (Fig. 1). The upper part of these sediments consists of calcarenites and conglomerates that form a phreatic aquifer separated from the Balanegra carbonate aquifer by a thick sequence of siltstones and marls. Close to the coast, the basement is elevated in an anticlinal that allows outcropping near to the Balanegra village (Marín-Lechado et al., 2005; Marín-Lechado and Pedrera, 2015).

3. Materials and methods

A sampling survey was carried out to monitor water quality and assess the main physico-chemical processes in the Balanegra aquifer. A total of 45 groundwater samples were taken from wells distributed in the study area (Fig. 1) to determine the major chemical components. In addition, temperature, electrical conductivity (EC) and pH were measured in situ. Alkalinity (as HCO_3) was determined by titration in-situ.

Samples were taken in duplicate and filtered with a 0.45 μm Millipore filter, collected into low density polyethylene bottles and stored at 4 °C. For cation analysis, 1 ml of ultra-pure nitric acid was added to prevent precipitation or absorption (Misstear et al., 2017).

Direct modeling is an important tool in the interpretation of the water-rock interaction processes. The mineral saturation indices (SI) indicate the degree of saturation in a particular mineral phase and based on this SI value, the trend of precipitation or dilution of the mineral phases can be deduced. For this reason, the PHREEQC code, version 3 (Parkhurst and Appelo, 2013) was used to evaluate the saturation indices of the water in calcite, dolomite, gypsum and halite. Geochemical simulations have been conducted under different scenarios. In this way, the calculated SI and calculated groundwater compositions were then compared to those of the analysed samples to deduce the process that best fitted the results.

Ionic deltas (Δ) were obtained for all the major ions based on the theoretical percentage of seawater, deduced from the concentration of the chloride ion. The concentration of an ion Y, by conservative mixing of seawater and freshwater is:

$$[Y]_m = [Y]_{sw} \cdot x + [Y]_{fw} \cdot (1 - x)$$

where $[Y]_m$ is the concentration of Y (conservative mixing), $[Y]_{sw}$ and $[Y]_{fw}$ are the end-members seawater and freshwater, x is fraction of seawater in the mixed water.

The value of the Δ ion is the difference between the measured concentration in the sample analysed and the theoretical value obtained deduced from ideal mixing between seawater and freshwater (Fidelibus et al., 1993; Pulido-Leboeuf, 2004.

In this way, ΔY is calculated as: $\Delta Y = [Y]_r - [Y]_m$ where, $[Y]_r$ is the actual value measured in the sample. The calculated ionic delta shows how far or close the ion concentration is from the theoretical value calculated for an ideal mixture. Positive delta values express enrichment, as a result of modifying process such as dissolution or ion exchange, whereas negative delta values indicate depletion of particular ions relative to a conservative mixing system. Values close to zero show that the ion has only been subjected to conservative mixing.

4. Results and discussion

4.1. Hydrochemical characterization

The analytical results obtained are summarized in Table 1. The

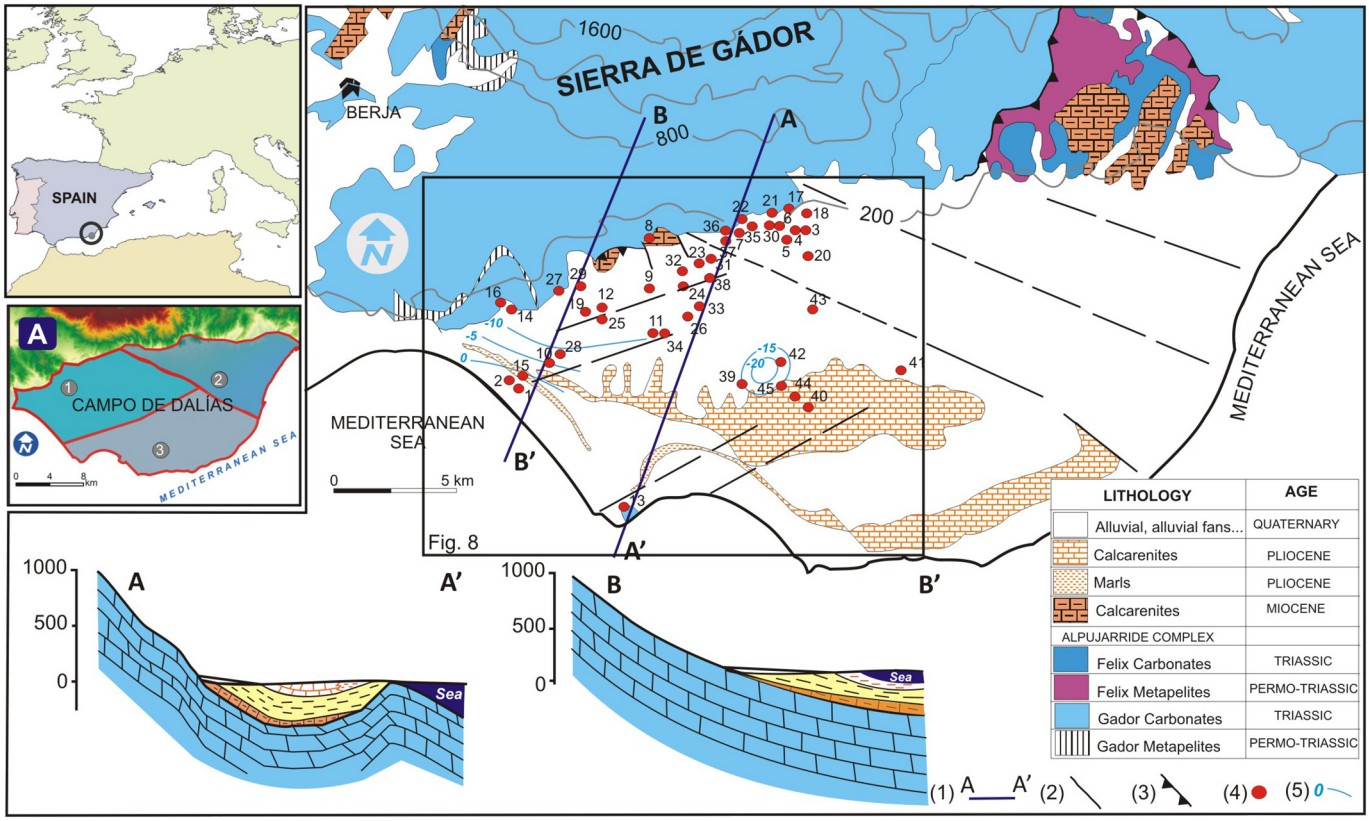

Fig. 1. Hydrogeological setting of the study area. (1) cross-section, (2) fault, (3) thrust fault, (4) sampling points (5) piezometric contours. Insert A: Location of the hydrogeological units in the Campo de Dalías (1: Aguadulce unit, 2: Balerma-Las Marinas unit, 3: Balanegra unit).

groundwater electrical conductivity (EC) show a wide range in salinity, from 414 μS/cm to 4080 μS/cm. The highest salinity corresponds to the samples taken close to the coastline, on the western limit of the study area. Groundwater temperature ranges between 20.5 °C and 40.6 °C. The higher thermal anomalies are related to the deeper pumping wells located in the central area of the aquifer. All the pH values where close to 7.5, ranging from 7.21 to 7.96.

The percentage of seawater in the samples was calculated from the chloride ion, according to the expression:

$$f_{SW} = \frac{[Cl_{sample}] - [Cl_f]}{[Cl_{sea}] - [Cl_f]} \times 100$$

where f_{SW} is the percentage of seawater, $[Cl_{sample}]$ is the concentration of Cl in the sample, $[Cl_{sea}]$ is the concentration of Cl in seawater, and $[Cl_f]$ is the concentration of Cl in freshwater. The results are presented in Table 1. These percentages range between 0.1 and 5%. According to these values, the waters can be classified between fresh and brackish water (Stuyfzand, 1989).

Analytical data were plotted on an expanded Durov diagram, where the cations and anions triangulate fields are separated along the 25% axes so that the main field is conveniently divided (Al-Bassam and Khalil, 2012; Al-Bassam et al., 1997). The distribution of the samples in this diagram shows four well-differentiated groups that will henceforth be referred to as G1 to G4 (Fig. 2). The G1 samples are characterized by HCO_3^- and Mg^{2+} as the dominant anion and cation, respectively. G2 has a similar composition, but samples were displaced towards the field of SO_4^{2-}. On the other hand, samples corresponding to groups G3 and G4 were characterized by their chloride content, but the G4 samples were more magnesic than G3. This differentiation of 45 samples into four groups, according to their content in major ions, is indicative of the main hydrogeochemical processes that influence the groundwater in the Balanegra aquifer.

In order to establish and identify all the processes that are active in the aquifer, different ionic ratios were calculated (Fig. 3). Comparing Cl^- and Na^+ ion concentration (Fig. 3a), it is observed that all the groups are aligned along the 1:1 line, which indicates halite dissolution. The Cl^- ion is a conservative ion in the water-rock interaction processes (Appelo and Postma, 2005), and the fact that all the samples are aligned along the 1:1 line would indicate that Na^+ ion follows the same pattern. Processes such as cation exchange or dissolution/precipitation of Na-bearing minerals other than halite can cause an increase or reduction in this cation compared to the expected values. However, all samples in the four groups show an increase in Na^+ content, following the same increasing trend as that of the Cl^- ion, thus providing evidence that none of these processes took place to a significant extent.

Given that dolomites and dolomitic limestones constitute the main rock in the Balanegra aquifer, the relationship between Cl and (Ca + Mg)-SO_4 is presented (Fig. 3b). This relationship revealed the carbonate dissolution processes without the influence of sulphate against the increase in salinity. Samples of groups G1, G2 and G3 show a clear alignment from the fresher values in G1 to the saltier in G3. All the samples of group G4 were however below this alignment, displaying a lower content of Ca and/or Mg cations, or a higher content of the SO_4 ion. To ascertain the cause of this differentiation between samples in G4 and the rest of the groups, Cl/Ca and Cl/Mg ratios were also plotted (Fig. 3c and d). In these graphs, the difference among the G4 samples and the other groups is very clear. In both diagrams, the G4 samples are aligned below the samples corresponding to G3. For Cl/Ca, the slope of the line representing G3 is approximately twice the slope of the line for G4. On the other side, the slope of G3 is three times that of G4 in the Cl/Mg graph.

4.2. Ionic deltas

The ionic delta values were calculated and are presented in Table 1.

Table 1
Physico-chemical data, ionic delta values (Δ), % seawater (SW) calculated from Cl ion and saturation indexes (SI) of the main mineral phases of the water samples collected from the Balanegra aquifer.

Sample	T	EC	pH	Cl	SO_4	HCO_3	NO_3	Na	Mg	Ca	K	ΔSO_4	ΔHCO_3	ΔNa	ΔMg	ΔCa	ΔK	% SW	$IS_{calcite}$	$IS_{dolomite}$	IS_{gypsum}	IS_{halite}	Group
	(° C)	μS/cm		meq/L								meq/L											
1	21,3	2380	7,50	13,48	9,23	3,40	0,00	12,55	9,65	6,44	0,28	7,79	−0,24	0,71	4,98	3,82	0,00	2,07	0,18	0,62	−1,04	−5,50	3
2	23,1	3780	7,29	29,96	4,96	3,80	0,00	18,37	13,84	8,60	0,58	1,94	0,21	−8,18	6,00	5,35	−0,03	4,81	0,15	0,62	−1,27	−5,01	3
3	26,4	638	7,50	3,00	0,89	4,08	0,33	2,47	2,75	2,37	0,09	0,47	0,41	−0,01	0,11	0,16	0,03	0,33	−0,40	−0,59	−2,18	−6,81	1
4	26,8	668	7,64	2,00	0,73	4,18	0,19	2,07	2,70	2,31	0,07	0,41	0,50	0,49	0,25	0,13	0,03	0,17	0,24	0,71	−2,26	−7,06	1
5	25,5	755	7,50	3,50	1,28	4,28	0,08	3,11	3,09	2,70	0,09	0,81	0,61	0,19	0,35	0,47	0,01	0,41	0,14	0,47	−1,99	−6,64	2
6	22,6	908	7,53	4,49	1,31	3,80	0,06	3,90	3,14	2,84	0,05	0,75	0,13	0,09	0,21	0,57	−0,05	0,58	0,09	0,33	−1,97	−6,43	2
7	24,0	574	7,40	2,00	0,91	3,76	0,10	1,82	2,67	2,23	0,07	0,59	0,08	0,23	0,23	0,06	0,03	0,17	−0,09	0,02	−2,17	−7,11	1
8	22,4	517	7,30	1,00	0,72	4,06	0,12	0,70	2,61	2,47	0,04	0,50	0,38	0,00	0,35	0,33	0,01	0,00	−0,12	−0,12	−2,21	−7,82	1
9	26,2	799	7,54	4,49	1,01	4,04	0,00	4,02	3,14	2,36	0,11	0,45	0,38	0,21	0,21	0,09	0,01	0,58	0,10	0,48	−2,15	−6,43	2
10	25,8	1113	7,55	5,99	1,53	4,10	0,07	4,18	4,34	3,23	0,09	0,82	0,44	−0,97	1,12	0,90	−0,03	0,83	0,22	0,71	−1,90	−6,29	3
11	24,2	1486	7,50	8,49	1,51	4,70	0,04	7,18	4,83	3,08	0,28	0,56	1,04	−0,20	1,13	0,66	0,10	1,24	0,17	0,66	−1,96	−5,91	3
12	25,8	992	7,43	6,49	0,99	4,16	0,11	4,78	3,86	3,05	0,11	0,24	0,50	−0,82	0,54	0,71	−0,02	0,91	0,09	0,43	−2,09	−6,20	3
13	30,8	4080	7,21	29,46	8,14	4,44	0,00	30,33	7,02	6,19	0,87	5,17	0,85	4,24	−0,73	2,97	0,27	4,73	0,08	0,41	−1,18	−4,82	4
14	25,4	1063	7,43	7,49	0,94	3,88	1,06	4,67	4,09	3,46	0,10	0,09	0,22	−1,82	0,58	1,08	−0,05	1,08	0,11	0,43	−2,08	−6,15	3
15	23,0	1833	7,52	10,48	6,57	3,40	0,00	9,07	7,59	5,42	0,15	5,42	−0,25	−0,09	3,50	2,92	−0,07	1,58	0,19	0,64	−1,20	−5,74	3
16	25,3	953	7,48	5,49	1,25	4,10	0,05	4,07	3,86	3,17	0,06	0,59	0,43	−0,64	0,74	0,86	−0,05	0,75	0,15	0,52	−1,97	−6,34	3
17	20,5	414	7,57	1,25	0,31	3,50	0,30	0,61	2,19	2,17	0,02	0,06	−0,18	−0,30	−0,11	0,03	−0,01	0,04	0,02	0,11	−2,59	−7,76	1
18	26,6	532	7,66	1,75	0,71	4,22	0,04	1,99	2,61	2,23	0,08	0,42	0,54	0,63	0,21	0,07	0,04	0,12	0,25	0,72	−2,28	−7,13	1
19	25,8	944	7,96	4,99	1,06	4,10	0,12	4,48	3,72	2,84	0,12	0,45	0,43	0,22	0,69	0,55	0,01	0,66	0,58	1,42	−2,08	−6,34	2
20	26,6	1913	7,51	16,48	1,19	4,13	2,96	14,07	4,04	3,63	0,39	−0,52	0,50	−0,44	−1,20	0,91	0,06	2,57	0,20	0,59	−2,04	−5,35	4
21	20,8	439	7,40	1,00	0,23	3,68	2,62	0,70	2,26	2,14	0,03	0,00	0,00	0,00	0,00	0,00	0,00	0,00	−0,13	−0,16	−2,74	−7,81	1
22	21,2	444	7,53	1,25	0,45	3,34	0,08	0,79	2,18	2,31	0,02	0,20	−0,34	−0,13	−0,12	0,16	−0,01	0,04	−0,01	0,04	−2,42	−7,66	1
23	25,7	905	7,61	5,49	1,19	3,90	0,36	4,67	3,27	2,65	0,13	0,53	0,23	−0,04	0,14	0,34	0,01	0,75	0,19	0,61	−2,05	−6,28	3
24	27,7	911	7,42	4,99	0,97	4,28	0,09	4,72	3,14	2,28	0,13	0,36	0,61	0,46	0,11	−0,01	0,03	0,66	−0,02	0,27	−2,20	−6,15	2
25	24,6	976	7,54	6,49	1,08	3,86	0,12	4,69	3,69	3,13	0,11	0,33	0,20	−0,91	0,37	0,78	−0,03	0,91	0,17	0,53	−2,04	−6,20	3
26	26,2	915	7,27	4,49	1,02	4,14	1,52	3,82	3,36	2,55	0,11	0,46	0,47	0,00	0,43	0,28	0,01	0,58	−0,12	0,02	−2,12	−6,45	2
27	25,0	802	7,50	4,49	1,22	4,22	0,11	3,26	3,52	3,30	0,08	0,66	0,55	−0,55	0,59	1,03	−0,02	0,58	0,20	0,56	−1,95	−6,52	2
28	25,6	1430	7,34	10,48	1,41	4,16	0,12	6,47	5,42	4,61	0,12	0,27	0,51	−2,70	1,34	2,11	−0,10	1,58	0,14	0,49	−1,85	−5,88	3
29	23,0	1163	7,50	7,49	1,12	4,18	0,28	4,67	4,48	3,77	0,05	0,27	0,52	−1,82	0,97	1,38	−0,10	1,08	0,20	0,59	−1,98	−6,15	3
30	24,6	1028	7,53	6,49	1,90	5,00	0,25	5,56	3,02	4,85	0,16	1,14	1,34	−0,04	−0,29	2,50	0,02	0,91	0,43	0,78	−1,65	−6,14	2
31	24,3	702	7,61	4,99	0,59	3,90	0,19	3,11	2,88	3,27	0,11	−0,02	0,23	−1,15	−0,15	0,98	0,00	0,66	0,28	0,63	−2,24	−6,49	3
32	23,3	586	7,49	2,50	0,86	3,78	0,11	1,35	3,00	2,71	0,04	0,49	0,10	−0,68	0,45	0,51	−0,01	0,25	0,07	0,29	−2,13	−7,14	1
33	28,8	1340	7,30	10,48	1,43	4,14	0,00	6,85	4,70	4,34	0,15	0,29	0,49	−2,32	0,61	1,84	−0,07	1,58	0,12	0,45	−1,86	−5,86	3
34	24,0	1528	7,59	8,99	1,50	4,64	0,38	7,05	5,77	2,50	0,17	0,50	0,98	−0,78	1,97	0,06	−0,01	1,33	0,15	0,80	−2,06	−5,90	3
35	25,2	840	7,71	4,49	0,97	4,48	0,00	4,61	2,91	2,62	0,12	0,41	0,81	0,80	−0,02	0,35	0,02	0,58	0,34	0,87	−2,13	−6,37	2
36	26,3	921	7,60	5,99	1,19	3,80	2,48	5,42	2,91	2,49	0,17	0,48	0,14	0,27	−0,31	0,17	0,04	0,83	0,15	0,52	−2,07	−6,18	4
37	24,9	496	7,37	1,25	0,62	3,71	0,16	1,54	2,33	1,97	0,06	0,37	0,03	0,63	0,03	−0,17	0,03	0,04	−0,15	−0,09	−2,36	−7,38	1
38	27,4	959	7,56	5,49	1,03	4,12	0,11	4,77	3,19	2,46	0,16	0,37	0,45	0,06	0,06	0,15	0,04	0,75	0,16	0,59	−2,14	−6,27	3
39	35,9	1964	7,36	13,98	3,70	3,84	0,00	13,96	3,50	3,34	0,28	2,22	0,20	1,68	−1,26	0,71	0,00	2,16	0,08	0,41	−1,60	−5,45	4
40	40,5	1420	7,65	7,99	1,75	3,84	0,00	7,98	2,95	2,70	0,21	0,85	0,18	1,04	−0,65	0,29	0,04	1,16	0,26	0,83	−2,12	−5,93	4
41	37,5	1325	7,62	20,97	1,86	3,70	0,00	19,00	3,28	4,02	0,23	−0,28	0,08	0,47	−2,84	1,12	−0,20	3,32	0,41	0,99	−1,84	−5,15	4
42	39,3	1570	7,78	12,98	1,86	3,58	0,00	11,36	3,41	3,40	0,24	0,48	−0,06	−0,03	−1,16	0,81	−0,02	1,99	0,54	1,34	−1,85	−5,57	4
43	35,0	1745	7,42	14,98	2,15	3,90	0,00	13,47	3,25	3,90	0,29	0,58	0,26	0,29	−1,70	1,23	−0,02	2,32	0,22	0,59	−1,75	−5,43	4
44	40,6	1508	7,36	10,99	1,74	3,70	0,00	8,84	3,42	3,86	0,21	0,55	0,05	−0,77	−0,77	1,34	−0,01	1,66	0,22	0,65	−1,82	−5,75	4
45	40,1	1474	7,39	13,98	1,68	3,70	0,00	11,40	3,52	4,41	0,21	0,20	0,06	−0,89	−1,24	1,78	−0,08	2,16	0,29	0,75	−1,81	−5,54	4
SW	17,0	55,000	7,93	603,48	58,09	110,01		538,28	118,43	24,95	12,05												

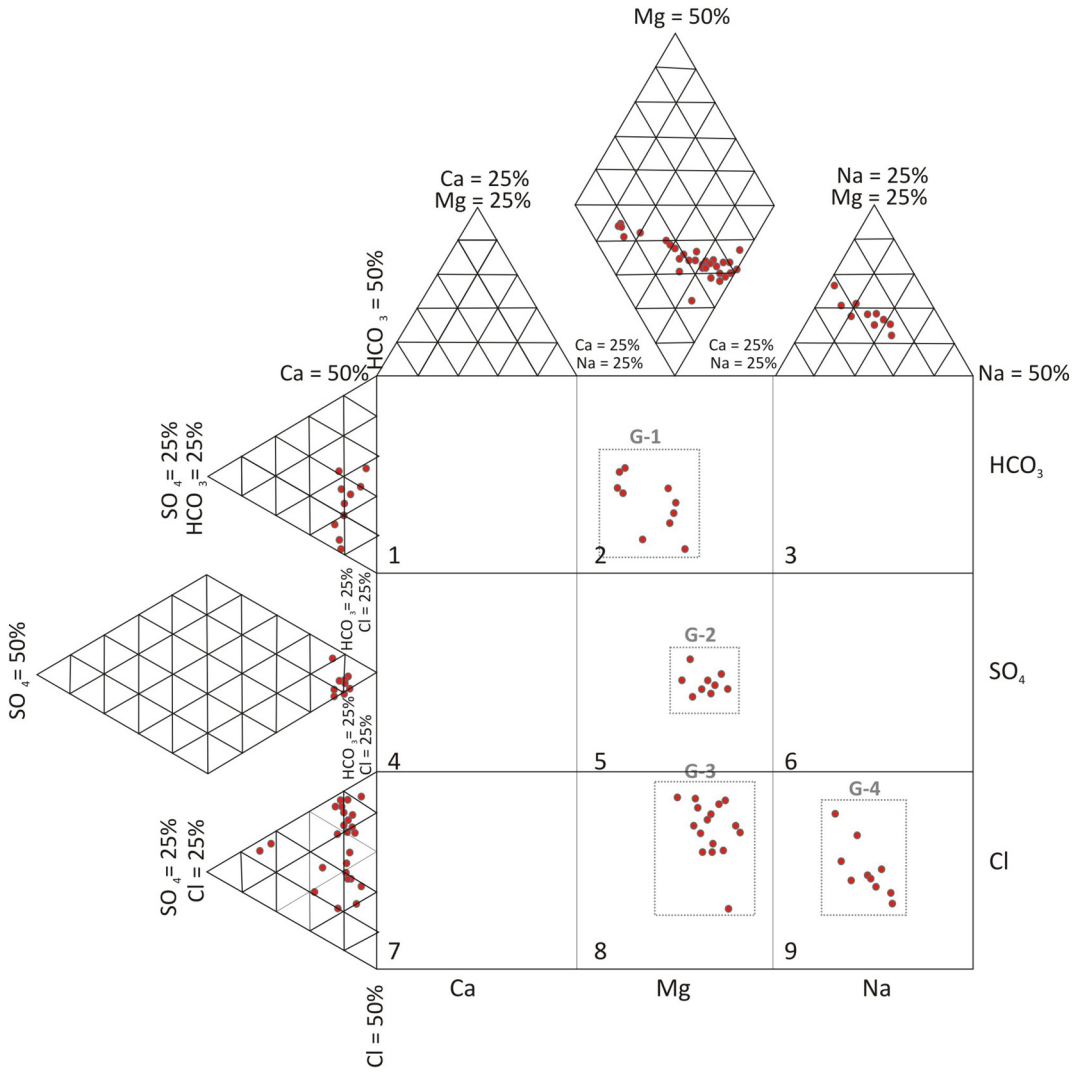

Fig. 2. Expanded Durov diagram of the groundwater samples.

The end-members to calculate delta values have been seawater and sample 21 from G1, corresponding to the fresher groundwater. The values of these deltas were positive for HCO_3 and SO_4 ions, whereas they were variable, positive and/or negative, for Na and K ions depending on the sample. The ionic deltas of Ca and Mg ions were differentiated by group (Fig. 4). Samples from G1 and G2, in general, had both cations enriched to the same extent. A similar pattern was observed for the G3 samples. In this group, the parallelism between the enrichment in Ca and Mg is more evident, and it is an indication that this enrichment is the result of the dissolution of dolomites. In contrast, the G4 samples follow a completely opposite trend. While there is a clear enrichment of the Ca ion, a reduction of the Mg ion occurs with the same magnitude as the Ca enrichment (Fig. 4).

The cause of this deficit in the magnesium ion in most saline samples (group G4) would be linked to an ion exchange process between Ca and Mg within the crystalline structure of the dolomite or magnesian limestone that composes the aquifer matrix. This cation exchange would be as a result of marine intrusion caused by pumping. The mixing of groundwater with a percentage of seawater increases the Mg concentration, favouring conditions for the latter to be fixed in the crystalline structure of the carbonates, by exchanging the Ca ion.

4.3. Mineral saturation indices

The saturation indices of the main mineral phases that can influence the chemical composition of the samples were calculated. These phases are dolomite and calcite, the main components in the aquifer matrix, along with gypsum and halite. Most groundwater in the Balanegra aquifer appeared to be in equilibrium or supersaturated with respect to calcite and dolomite, as the SIs with respect to these minerals were close to zero or positive (Fig. 5). In contrast, all sampled groundwater had negative saturation indices with respect to gypsum and halite, meaning they were undersaturated.

The saturation index in dolomite was positive in most of the samples, displaying values of up to 1.4. It was only negative in the G1 samples that were less mineralized, which is similar to what was observed for SI in calcite. Some of the G2 samples displayed the highest SI values in these carbonates. The SI in gypsum ranged between −2.7 and −1, meaning this phase would be susceptible to dissolution if it were located in an aquifer matrix. The distribution of the samples followed a curve along which the most saline samples are those SI that are less negative. Similar results were found for the SI in halite, albeit the curve fit was better (Fig. 5).

4.4. Modeling

To elucidate the main processes that are active in this aquifer, the field data were compared in a model to the experimental results using the PHREEQC code. The steady-state is an assumption used in modeling of the chemical evolution in the groundwater system. More sampling

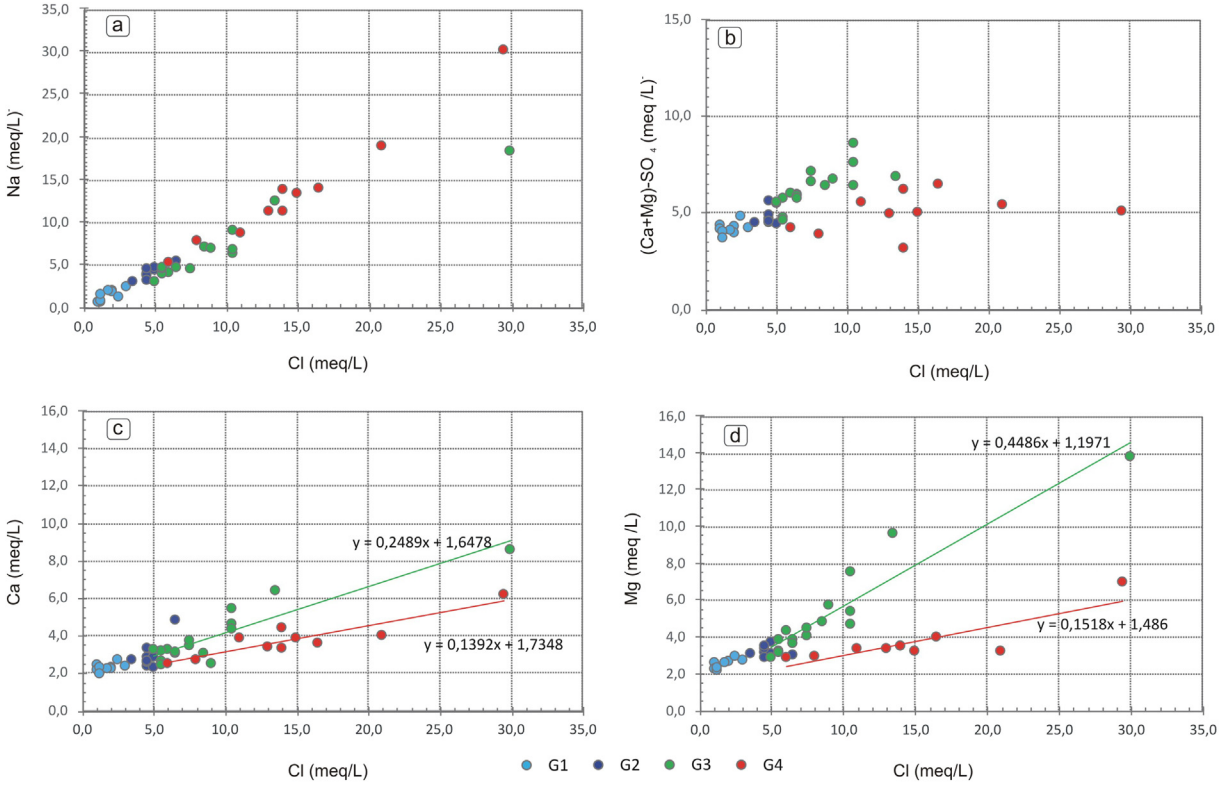

Fig. 3. Hydrochemical relationships between concentrations of major ions and conservative ion Cl (data in meq/L).

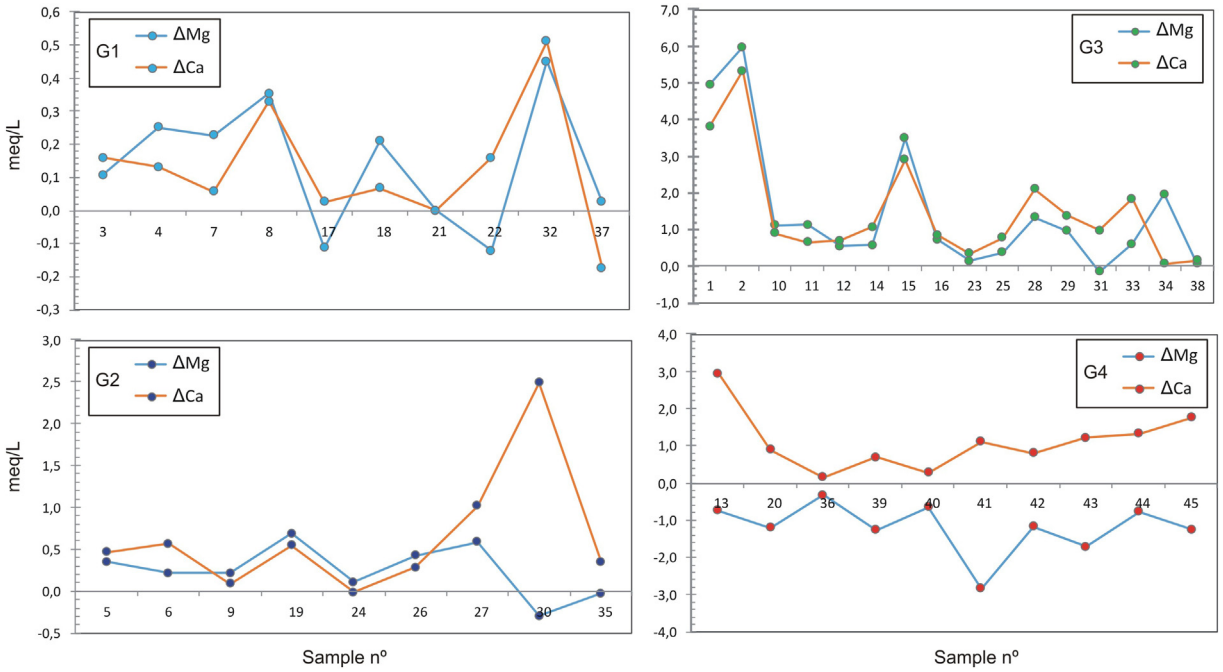

Fig. 4. Ionic Deltas for Ca and Mg ions corresponding to the samples in groups G1 to G4.

campaigns should be necessary to identify temporal fluctuations that the aquifer can likely to experience.

Based on the percentages of seawater and the ion deltas calculated (Table 1), a simulation was conducted to obtain the expected ionic concentrations of the samples from groups G3 and G4, which featured greater compositional variability than G1 and G2, with respect to ionic relationships Cl/Mg and Cl/Ca (Fig. 6). The values obtained correspond quite accurately to the average values in each of the samples. These figures also include a line representing the theoretical freshwater-seawater mixture. As for the Cl/Mg relationship, this straight line is located above all the measured and simulated samples of G4 and below those of G3. With regard to the Cl/Ca graph, the theoretical freshwater-seawater line falls below both groups of samples, albeit G3 was much farther from the mixture line than G4 (Fig. 6).

Additionally, the SI values were modeled for the four most important mineral phases, i.e. calcite, dolomite, gypsum and halite

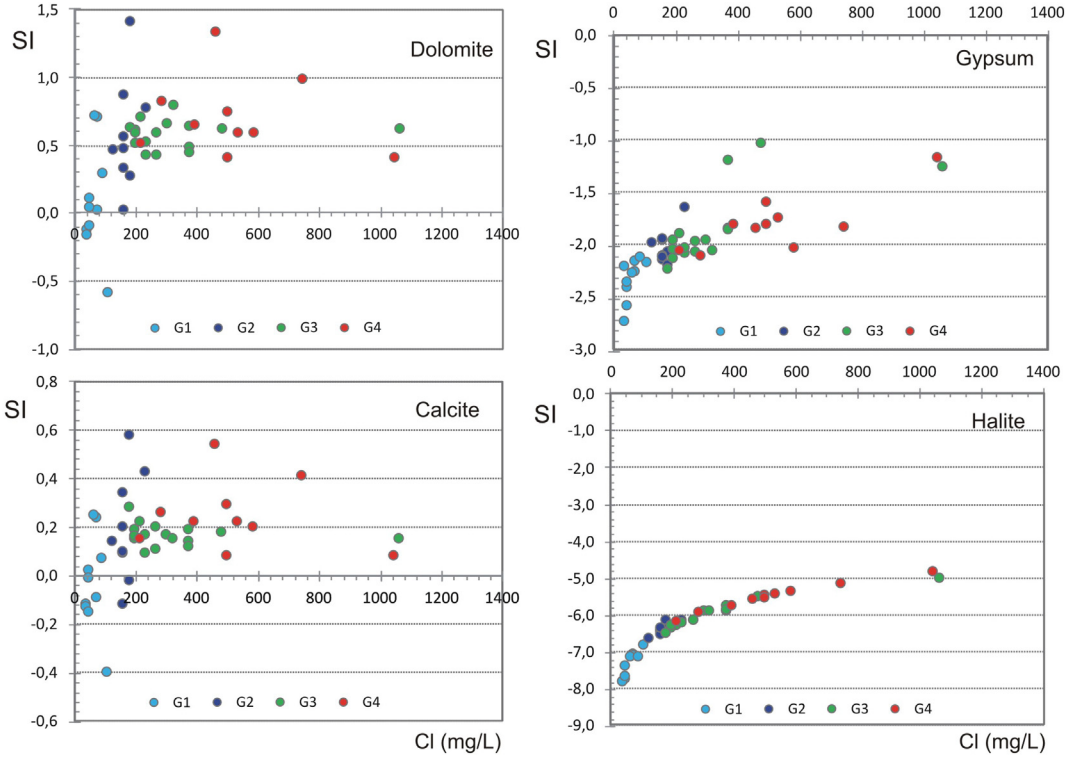

Fig. 5. Saturation indexes of calcite, dolomite, gypsum and halite in sampled water versus chloride concentration in mg/L.

(Fig. 7). In these simulations, the starting point was established by sample G1, which featured very low mineralization. During the first stage of modeling, calcium-magnesium-carbonate was increased to simulate the dissolution of dolomite, and calcium-sulphate was increased to simulate the dissolution of gypsum (Fig. 7). Consequently, the SIs in calcite, dolomite and gypsum increase substantially, fitting the simulation curve quite well to the SI values measured. After a certain point, due to the effect the common ion, calcite tends to precipitate, causing the SIs in calcite and dolomite to decrease, while the values for gypsum remain the stable. Finally, the mixture of the resulting sample in the last stage combined with seawater was simulated. The simulation values aligned with the values measured for the G4 samples.

Simulations were also conducted for the SIs that would be obtained in the samples if there had only been one freshwater-seawater mixing process. Only in the case of the SI for halite was a good fit observed. The lack of a fit for the remaining mineral phases, with the curve representing the freshwater-seawater mixture, indicates that other geochemical processes must have been at work.

4.5. Hydrochemical processes

A series of interpretations of the key hydrochemical processes at work in the dolomite coastal aquifer of Balanegra can be made based on analyses of the main physico-chemical components, the results of the ionic deltas and the mineral saturation indices.

The dissolution of the dolomite rock was the main mineralization process of the groundwater, especially in the G1 samples. Consequently, the recharge water from rainfall gradually increased its Ca and Mg content. The concentrations in these two cations increased in parallel in this group. Regarding the samples corresponding to G2, there was a

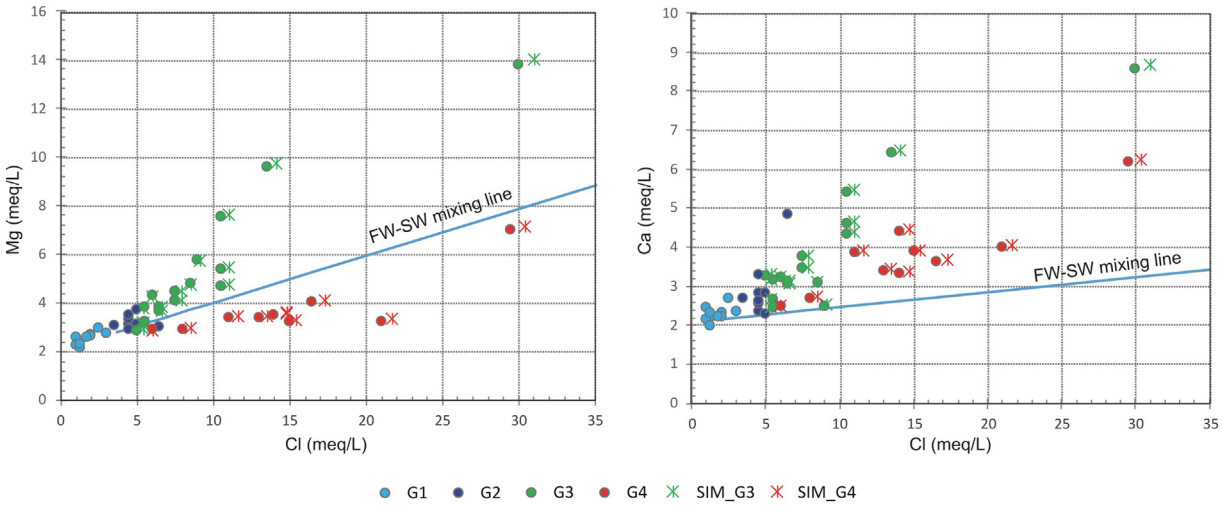

Fig. 6. Cl/Mg and Cl/Ca ratios. Comparison between measured and simulated concentrations for samples in groups G3 and G4 (data in meq/L).

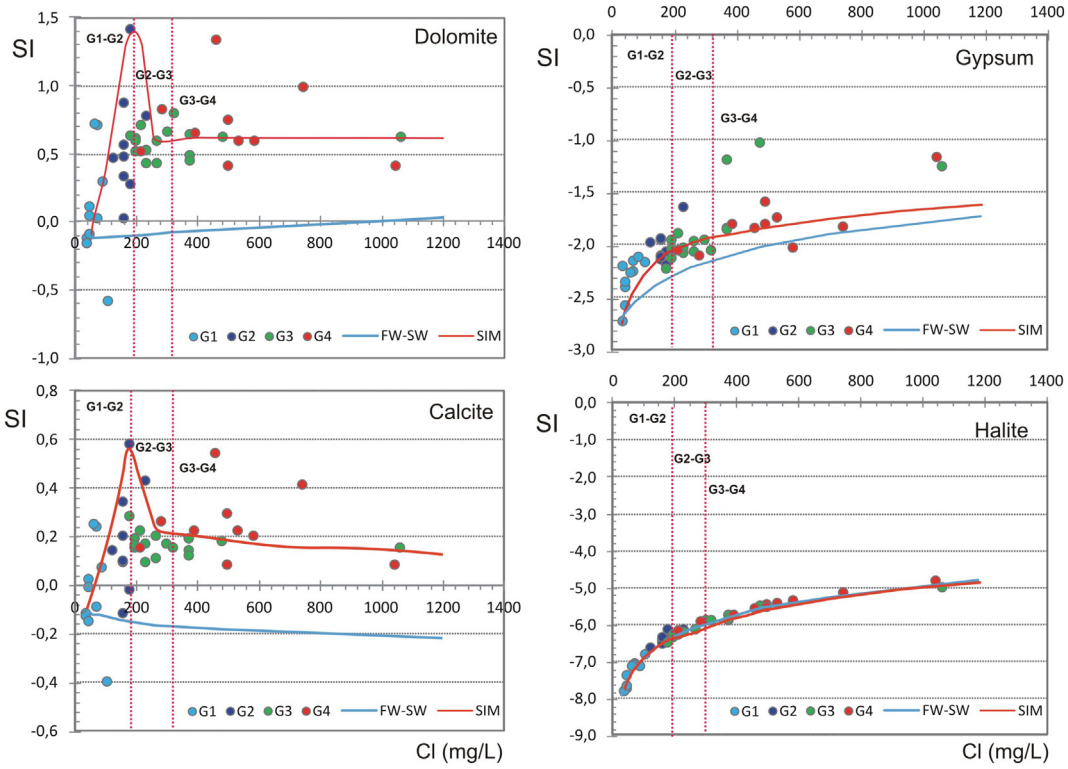

Fig. 7. Saturation Index (SI) with respect to dolomite, gypsum, calcite and halite versus chloride concentration in mg/L. The red line corresponds to SI according to the geochemical simulation with PHREEQC (SIM). The line (blue) of theoretical SI in a conservative freshwater–seawater mix is also plotted (FW-SW). (For interpretation of the references to color in this figure legend, the reader is referred to the web version of this article.)

slightly greater proportion of Mg than Ca (Table 1, Fig. 3). The content of SO_4 was also higher as a result of the dissolution of gypsum. The presence of interstratified gypsum between the layers of dolomites in the aquifer is relatively common (Martín-Rojas et al., 2007, 2012). The magnesium concentration in groundwater is an indication that dolomite and high magnesium calcite may be present in the aquifer. The dissolution of dolomite by calcite-saturated groundwater generally occurs incongruently, i.e. calcite is precipitated as the dolomite is dissolved. This effect has been described in many carbonate aquifers (Wigley, 1973; Palmer and Cherry, 1984; Cardenal et al., 1994; Moral et al., 2008). The result of this process is an increase in the concentration of bicarbonate and magnesium ions and a slight decrease in Ca.

G3 samples were characterized by having a higher salinity than G2. The wells where these samples were taken were relatively deep. They pass through an upper detrital aquifer, highly contaminated by the agricultural activity (Foster et al., 2018) conducted in the surrounding area, and layers of silt and clay, which confines the carbonate aquifer. The increase in salinity detected in the G3 samples would most likely be due to the contribution of more saline water coming from the upper aquifer, resulting from the poorly designed construction of some of these wells. This superficial contamination is reflected in the high content of NO_3 present in these samples (Table 1). As for the G4 samples, they were also characterized by a higher salinity, but in this case there was no presence of nitrates.

By plotting the aquifer points where the samples were taken on a map, and indicating the group to which they belong (Fig. 8), it can be observed that the samples corresponding to G1 and G2 are, in general, the closest to the edge of the Sierra de Gádor, while G3 and G4 are located in the central and coastal zone of the aquifer. However, whereas G3 is distributed more towards the northern part of the aquifer, G4 is distributed towards the southern part of the aquifer (Fig. 8).

This distribution of the G3 and G4 samples is controlled by the general structure of the aquifer. The dolomite rocks extend from the

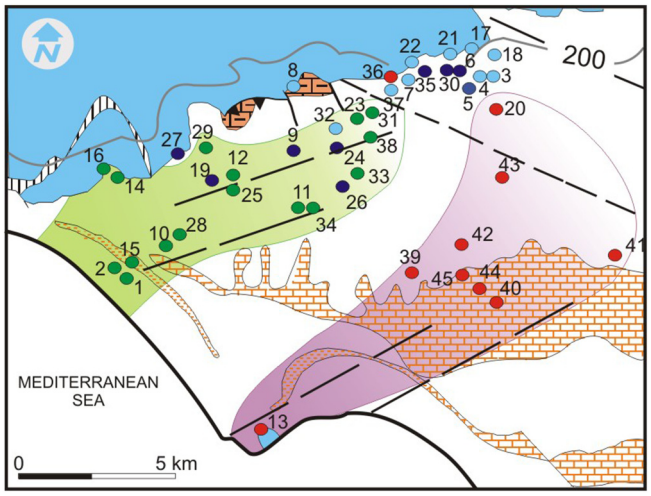

Fig. 8. Distribution of the samples according to the groups identified in the study.

edge of the Sierra de Gádor, progressively deepening below the thick Neogene sedimentary sequence that confines the carbonates. They follow a fold geometry that runs from synform type to antiform, forming the carbonated rocks at the far southern end of the aquifer (Figs. 1 to 8). This small outcrop of dolomite rocks on the southern coastline is responsible for the geochemical differences observed between the G3 and G4 samples. At this site, contact between the aquifer and the sea is possible, but this connection does not exist along the rest of the coastline. It is through this connection that a seawater intrusion process would have taken place, which would have salinized the G4 samples, exacerbated by the intense groundwater abstraction in this area. As a result of this seawater intrusion, waters rich in Mg enter the

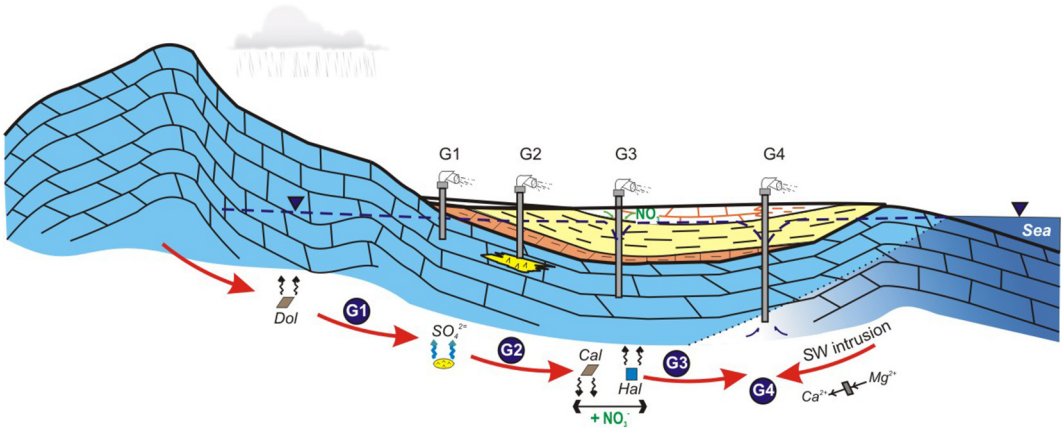

Fig. 9. Conceptual model of the main hydrogeochemical processes recognized in the study area.

aquifer system. This magnesium would have exchanged in the crystalline structure of the dolomite and magnesian limestone, releasing Ca ions. Consequently, the ionic deltas are positive for Ca and negative for Mg in the samples of this group (Table 1, Fig. 4). The formation of a calcite-magnesite solid solution is induced by the high Mg:Ca ratio of intruding seawater according to the following reaction:

$$Ca_xMg_{(1-x)}CO_3 + yMg^{2+} \rightarrow Ca_{x-y}Mg_{(1-x+y)}CO_3 + yCa^{2+}$$

As a result, Ca is added while Mg is removed from groundwater. This rock-water interaction process intensifies the impact of cation exchange (Ca surplus vs. Mg deficit) along the flow path of the dolomitic limestone. The Mg deficit induces Mg desorption and causes a lower fraction of exchangeable Mg in the salinized zone compared to the freshwater zone (Khadra et al., 2017). A summary of the main hydrochemical processes at work in the aquifer is depicted in Fig. 9.

The cation exchange processes linked to marine intrusion is usually dominated by Na (Appelo and Postma, 2005; Andersen et al., 2005; Sivan et al., 2005). Nevertheless, the ion exchange Ca-Mg has hardly been identified in other areas with carbonate sediments (Appelo, 1994; Khadra et al., 2017; Behera et al., 2019). According to Burt (1993), dolomite is equivalent, in terms of mass balance, to pure calcite in which magnesium has been substituted for half the calcium, as in a cation exchange reaction. Dissolution of dolomite can, therefore, be represented in the mass balance problem as a combination of calcite dissolution and cation exchange as follows, where y is an exchange site:

$$2CaCO_3 \leftrightarrow 2Ca^{2+} + 2CO_3$$

$$yMg + Ca^{2+} \leftrightarrow yCa + Mg^{2+}$$

5. Conclusions

Over the past several decades, the carbonated aquifer of Balanegra has been experiencing salinization in the central and coastal sectors as a result of intense groundwater abstraction. Of the four groups of samples that were analysed, those corresponding to groups G3 and G4 were affected by salinization. However, the causes of the salinization in G3 and G4 differ, as revealed by the chemical analysis of their waters. The main cause of salinization in G3 was the salinization from the upper detrital aquifer through the wells themselves. The upper aquifer is currently salinized as a result of irrigation return-flow, as well as the presence of salts in the detrital formations. As for G4, there are clear signs indicating that it was salinized exclusively through seawater intrusion. The hydrochemical processes that take place in the aquifer are varied and do not act in isolation; instead, they act at the same time and with different intensity, which is more evident in areas of higher salinity. The Ca/Mg cation exchange in dolomites and magnesic limestone of coastal carbonated aquifers would be one of the hydrochemical processes most directly linked to these seawater intrusion processes. The ionic deltas of Ca and Mg in coastal carbonated aquifers allow us to recognize whether the salinity of the samples is the result of the seawater intrusion process, in which case positive ΔCa values and negative ΔMg values would be expected. The intensive exploitation of the groundwater has led to a generalized drop in water levels and a concomitant deterioration of water quality observed in samples G-3 and G-4. Consequently, the volume of usable groundwater is reduced, showing the need of a better management of this aquifer to ensure its future sustainability.

Authors' statement

Angela Vallejos: Writing - Review & Editing
Linda Daniele: Formal Analysis
Fernando Sola: Conceptualization, Methodology
Luís Molina: Investigation
Antonio Pulido-Bosch: Project administration

Declaration of competing interest

The authors declare that they have no known competing financial interests or personal relationships that could have appeared to influence the work reported in this paper.

Acknowledgements

This work formed part of the general research activities promoted by the CEI-MAR Campus of International Excellence and it was supported by MINECO and FEDER, through Project CGL2015-67273-R. Part of the survey work was also been funded by the Regular FONDECYT, Project No. 1170569.

References

Al-Bassam, A.M., Khalil, A.R., 2012. DurovPwin: a new version to plot the expanded Durov diagram for hydro-chemical data analysis. Comput. Geosci. 42, 1–6.
Al-Bassam, A.M., Awad, H.S., Al-Alawi, J.A., 1997. DurovPlot a computer program for processing and plotting hydro-chemical data. Groundwater 35 (2), 362–367.
Alcalá, F.J., Custodio, E., 2008. Using the Cl/Br ratio as a tracer to identify the origin of salinity in aquifers in Spain and Portugal. J. Hydrol. 359, 189–207.
Andersen, M.S., Nyvang, V., Jakobsen, R., Postma, D., 2005. Geochemical processes and solute transport at the seawater/freshwater interface of a sandy aquifer. Geochim. Cosmochim. Acta 69 (16), 3979–3994.
Appelo, C.A.J., 1994. Cation and proton exchange, pH variations, and carbonate reactions in a freshening aquifer. Water Resour. Res. 30, 2793–2805.
Appelo, C.A.J., Postma, D., 2005. Geochemistry, Groundwater and Pollution, 2nd ed. A.A. Balkema, Leiden, The Netherlands (649 pp).
Barbieri, M., Boschetti, T., Petitta, M., Tallini, M., 2005. Stable isotopes (^2H, ^{18}O and $^{87}Sr/^{86}Sr$) and hydrochemistry monitoring for groundwater hydrodynamics analysis in a karst aquifer (Gran Sasso, Central Italy). Appl. Geochem. 20, 2063–2081.
Bear, J., 2004. Management of a coastal aquifer. Groundwater 42, 317.

Behera, A.K., Chakrapani, G.J., Kumar, S., Rai, N., 2019. Identification of seawater intrusion signatures through geochemical evolution of groundwater: a case study based on coastal region of the Mahanadi delta, Bay of Bengal, India. Nat. Hazards 97, 1209–1230.
Burak, S., Doğan, E., Gazioğlu, C., 2004. Impact of urbanization and tourism on coastal environment. Ocean Coast. Manag. 47, 515–527.
Burt, R.A., 1993. Ground-water chemical evolution and diagenetic processes in the Upper Floridan Aquifer, southern South Carolina and northeastern Georgia. In: USGS Report, (76 pp).
Campana, C., Fidelibus, M.D., 2015. Reactive-transport modelling of gypsum dissolution in a coastal karst aquifer in Puglia, southern Italy. Hydrogeol. J. 23, 1381–1398.
Cardenal, J., Benavente, J., Cruz-Sanjulián, J.J., 1994. Chemical evolution of groundwater in triassic gypsum-bearing carbonate aquifers (Las Alpujarras, southern Spain). J. Hydrol. 161, 3–30.
Carreira, P.M., Marques, J.M., Nunes, D., 2014. Source of groundwater salinity in coastline aquifers based on environmental isotopes (Portugal): natural vs. human interference – a review and reinterpretation. Appl. Geochem. 41, 163–175.
Cary, L., Petelet-Giraud, E., Bertrand, G., Kloppmann, W., Aquilina, L., Martins, V., Hirata, R., Montenegro, S., Pauwels, H., Chatton, E., Franzen, M., Aurouet, A., 2015. Origins and processes of groundwater salinization in the urban coastal aquifers of Recife (Pernambuco, Brazil): a multi-isotope approach. Sci. Total Environ. 530–531, 411–429.
Caschetto, M., Colombani, N., Mastrocicco, M., Petitta, M., Aravena, R., 2016. Estimating groundwater residence time and recharge patterns in a saline coastal aquife. Hydrol. Process. 30 (22), 4202–4213.
Changming, L., Jingjie, Y., Kendy, E., 2001. Groundwater exploitation and its impact on the environment in the North China Plain. Water Int. 26, 265–272.
Chowdhury, A.H., Scanlon, B.R., Reedy, R.C., Young, S., 2018. Fingerprinting groundwater salinity sources in the Gulf Coast Aquifer System, USA. Hydrogeol. J. 26, 197–213.
Colombani, N., Osti, A., Volta, G., Mastrocicco, M., 2016. Impact of climate change on salinization of coastal water resources. Water Resour. Manag. 30, 2483–2496.
Custodio, E., Bruggeman, G.A., 1987. Groundwater problems in coastal areas. In: Studies and Reports in Hydrology No. 45. UNESCO, Paris (576 pp).
Custodio, E., Andreu-Rodes, J.M., Aragón, R., Estrela, T., Ferrer, J., García-Aróstegui, J.L., Manzano, M., Rodríguez-Hernández, L., Sahuquillo, A., del Villar, A., 2016. Groundwater intensive use and mining in south-eastern peninsular Spain: Hydrogeological, economic and social aspects. Sci. Total Environ. 559, 302–316.
Daniele, L., Vallejos, A., Corbella, M., Molina, L., Pulido-Bosch, A., 2013. Geochemical simulations to assess water–rock interactions in complex carbonate aquifers: the case of Aguadulce (SE Spain). Appl. Geochem. 29, 43–54.
Du, Y., Ma, T., Chen, L., Shan, H., Xiao, C., Lu, Y., Liu, C., Cai, H., 2015. Genesis of salinized groundwater in Quaternary aquifer system of coastal plain, Laizhou Bay, China: Geochemical evidences, especially from bromine stable isotope. Appl. Geochem. 59, 155–165.
Edmunds, W.M., 2001. Paleowater in European coastal aquifers – the goals and main conclusions of the PALAEAUX project. In: Edmunds, W.M., Milne, C.J. (Eds.), Paleowaters in Coastal Europe: Evolution of Groundwater since the Late Pleistocene. Geological Society Special Publication, pp. 1–16.
Ferguson, G., Gleeson, T., 2012. Vulnerability of coastal aquifers to groundwater use and climate change. Nat. Clim. Chang. 2, 342–345.
Fidelibus, M.D., Giménez, E., Morell, I., Tulipano, L., 1993. Salinization processes in the Castellon Plain aquifer. In: Study and Modelling of Saltwater Intrusion into Aquifers. CIMNE-UPC, Barcelona, pp. 267–283.
Foster, S., Pulido-Bosch, A., Vallejos, A., Molina, L., Llop, A., Macdonald, A.M., 2018. Impact of irrigated agriculture on groundwater-recharge salinity: a major sustainability concern in semi-arid regions. Hydrogeol. J. 26 (8), 2781–2791.
Gattacceca, J.C., Vallet-Coulomb, C., Mayer, A., Claude, C., Radakovitch, O., Conchetto, E., Hamelin, B., 2009. Isotopic and geochemical characterization of salinization in the shallow aquifers of a reclaimed subsiding zone: the southern Venice Lagoon coastland. J. Hydrol. 378 (1–2), 46–61.
Gomes, O.V.O., Marques, E.D., Kütter, V.T., Aires, J.R., Travi, Y., Silva-Filho, E.V., 2019. Origin of salinity and hydrogeochemical features of porous aquifers from northeastern Guanabara Bay, Rio de Janeiro, SE - Brazi. Journal of Hydrology: Regional Studies 22, 100601.
González-Baheza, A., Arizpe, O., 2018. Vulnerability assessment for supporting sustainable coastal city development: a case study of La Paz, Mexico. Clim. Dev. 10 (6), 552–565.
Gorelick, S.M., Zheng, C., 2015. Global change and the groundwater management challenge. Water Resour. Res. 3031–3051.
Khadra, W.M., Stuyfzand, P.J., van Breukelen, B.M., 2017. Hydrochemical effects of saltwater intrusion in a limestone and dolomitic limestone aquifer in Lebanon. Appl. Geochem. 79, 36–51.
Liu, Y., Jiao, J.J., Liang, W., Kuang, X., 2017. Hydrogeochemical characteristics in coastal groundwater mixing zone. Appl. Geochem. 85, 49–60.
Marín-Lechado, C., Pedrera, A., 2015. Smooth folds favoring gypsum precipitation in the Messinian Poniente marginal basin (Western Mediterranean). Tectonophysics 663, 48–61.
Marín-Lechado, C., Galindo-Zaldívar, J., Rodríguez-Fernández, L.R., Serrano, I., Pedrera, A., 2005. Active faults, seismicity and stresses in an internal boundary of a tectonic arc (Campo de Dalías and Níjar, southeastern Betic Cordilleras, Spain). Tectonophysics 396, 81–96.
Martín-Rojas, I., Estévez Rubio, A., Delgado Salazar, F., 2007. Tectonic units and general structure of the Sierra de Gádor and surrounding areas (Betic Cordillera, Almería province): Palaeogeographic implications. Estudios Geologicos 63, 27–42.
Martín-Rojas, I., Somma, R., Delgado, F., Estevez, A., Iannace, A., Zamparelli, V., 2012. The Triassic platform of the Gador-Turon unit (Alpujarride complex, Betic Cordillera, southeast Spain): climate versus tectonic factors controlling platform architecture. Facies 58, 297–323.
Misstear, B., Banks, D., Clark, L., 2017. Water Wells and Boreholes, 2nd edition. John Wiley & Sons Inc, Hoboken, NJ.
Molina, L., Vallejos, A., Pulido-Bosch, A., Sánchez-Martos, F., 2002. Water temperature and conductivity variability as indicators of groundwater behaviour in complex aquifer systems in the south-east of Spain. Hydrol. Process. 16, 3365–3378.
Mollema, P., Antonellini, M., Dinelli, E., Gabbianelli, G., Greggio, N., Stuyfzand, P., 2013. Hydrochemical and physical processes influencing salinization and freshening in mediterranean low-lying coastal environments. Appl. Geochem. 34, 207–221.
Moral, F., Cruz-Sanjulián, J.J., Olias, M., 2008. Geochemical evolution of groundwater in the carbonate aquifers of Sierra de Segura (Betic Cordillera, southern Spain). J. Hydrol. 360, 281–296.
Palmer, C.D., Cherry, J.A., 1984. Geochemical evolution of groundwater in sequences of sedimentary rocks. J. Hydrol. 75, 27–65.
Parkhurst, D.L., Appelo, C.A.J., 2013. Description of input and examples for PHREEQC versión 3—a computer program for speciation, batch-reaction, one-dimensional transport, and inverse geochemical calculations. In: U.S. Geological Survey Techniques and Methods, book 6, chap. A43, 497 p., available only at. http://pubs.usgs.gov/tm/06/a43/.
Pulido-Bosch, A., 2005. Recharge in the Sierra de Gador and Hydrogeochemistry of the Campo de Dalias Aquifers (in Spanish). Report. Cajamar Experimental Station, Almeria (337 pp).
Pulido-Bosch, A., Navarrete, F., Molina, L., Martínez-Vidal, J.L., 1992. Quantity and quality of groundwater in the Campo de Dalías (Almería, SE Spain). Water Sci. Technol. 24 (11), 87–96.
Pulido-Bosch, A., Rigol-Sánchez, J.P., Vallejos, A., Andreu, J.M., Cerón, J.C., Molina-Sánchez, L., Sola, F., 2018. Impacts of agricultural irrigation on groundwater salinity. Environ. Earth Sci. 77, 197.
Pulido-Leboeuf, P., 2004. Seawater intrusion and associated processes in a small coastal complex aquifer (Castell de Ferro, Spain). Appl. Geochem. 19, 1517–1527.
Raidla, V., Kirsimäe, K., Vaikmäe, R., Jõeleht, A., Karro, E., Marandi, A., Savitskaja, L., 2009. Geochemical evolution of groundwater in the Cambrian-Vendian aquifer system of the Baltic Basin. Chem. Geol. 258, 219–231.
Russak, A., Sivan, O., 2010. Hydrogeochemical tool to identify salinization or freshening of coastal aquifers determined from combined field work, experiments, and modeling. Environmental Science & Technology 44, 4096–4102.
Sánchez-Martos, F., Pulido-Bosch, A., Molina-Sánchez, L., Vallejos-Izquierdo, A., 2002. Identification of the origin of salinization in groundwater using minor ions (Lower Andarax, Southeast Spain). Sci. Total Environ. 297, 43–58.
Scheiber, L., Ayora, C., Vázquez-Suñé, E., Cendón, D., Soler, A., Custodio, E., Baquero, J.C., 2015. Recent and old groundwater in the Niebla-Posadas regional aquifer (southern Spain): implications for its management. J. Hydrol. 523, 624–635.
Shi, L., Jiao, J.J., 2014. Seawater intrusion and coastal aquifer management in China: a review. Environ. Earth Sci. 72, 2811–2819.
Sivan, O., Yechieli, Y., Herut, B., Lazar, B., 2005. Geochemical evolution and timescale of seawater intrusion into the coastal aquifer of Israel. Geochim. Cosmochim. Acta 69, 579–592.
Sola, F., Vallejos, A., Moreno, L., López Geta, J.A., Pulido Bosch, A., 2013. Identification of hydrogeochemical process linked to marine intrusion induced by pumping of a semiconfined mediterranean coastal aquifer. Int. J. Environ. Sci. Technol. 10, 63–76.
Sola, F., Vallejos, A., Daniele, L., Pulido-Bosch, A., 2014. Identification of a Holocene aquifer-lagoon system using hydrogeochemical data. Quat. Res. 82, 121–131.
Stuyfzand, P.J., 1989. A New Hydrochemical Classification of Watertypes. 182. IAHS Publ, pp. 89–98.
Sukhija, B.S., Varma, V.N., Nagabhushanam, P., Reddy, D.V., 1996. Differentiation of palaeomarine and modern seawater intruded salinities in coastal groundwaters (of Karaikal and Tanjavur, India) based on inorganic chemistry, organic biomarker fingerprints and radiocarbon dating. J. Hydrol. 174, 173–201.
Tran, L.T., Larsen, F., Pham, N.Q., Christiansen, A.V., Tran, N., Vu, H.V., Tran, L.V., Hoang, H.V., Hinsby, K., 2012. Origin and extent of fresh groundwater, salty paleowaters and recent saltwater intrusions in Red River flood plain aquifers, Vietnam. Hydrogeol. J. 20, 1295–1313.
Vallejos, A., Díaz-Puga, M.A., Sola, F., Daniele, L., Pulido-Bosch, A., 2015. Using ion and isotope characterization to delimitate a hydrogeological macrosystem. Sierra de Gádor (SE, Spain). J. Geochem. Explor. 155, 14–25.
Vallejos, A., Sola, F., Yechieli, Y., Pulido-Bosch, A., 2018. Influence of the paleogeographic evolution on the groundwater salinity in a coastal aquifer. Cabo de Gata aquifer, SE Spain. J. Hydrol. 557, 55–66.
Vengosh, A., Spivack, A.J., Artzi, Y., Ayalon, A., 1999. Geochemical and boron, strontium, and oxygen isotopic constraints on the origin of the salinity in groundwater from the Mediterranean coast of Israel. Water Resour. Res. 35, 1877–1894.
Vengosh, A., Kloppmann, W., Marei, A., Livshitz, Y., Gutierrez, A., Banna, M., Guerrot, C., Pankratov, I., Raanan, H., 2005. Sources of salinity and boron in the Gaza strip: Natural contaminant flow in the southern Mediterranean coastal aquifer. Water Resour. Res. 41, 1–19.
Werner, A.D., Jakovovic, D., Simmons, C.T., 2009. Experimental observations ofsaltwater up-coning. J. Hydrol. 373, 230–241.
Werner, A.D., Ward, J.D., Morgan, L.K., Simmon, C.T., Robinson, N.I., Teubner, M.D., 2012. Vulnerability indicators of seawater intrusion. Groundwater 50, 48–58.
Werner, A.D., Bakker, M., Post, V.E.A., Vandenbohede, A., Lu, C., Ataie-Ashtiani, B., Simmons, C.T., Barry, D.A., 2013. Seawater intrusion processes, investigation and management: recent advances and future challenges. Adv. Water Resour. 5, 3–26.
Wigley, T.M.L., 1973. The incongruent solution of dolomite. Geochim. Cosmochim. Acta 37, 1397–1402.
Yechieli, Y., Yokochi, R., Zilberbrand, M., Lu, Z.T., Purtschert, R., Sueltenfuss, J., Jiang, W., Zappala, J., Mueller, P., Bernier, R., Avrahamov, N., Adar, E., Talhami, F., Livshitz, Y., Burg, A., 2019. Recent seawater intrusion into deep aquifer determined by the radioactive noble-gas isotopes ^{81}Kr and ^{39}Ar. Earth Planet. Sci. Lett. 507, 21–29.